Experimental study of the diffusion of Xe and Kr implanted at low concentrations in UO2 and determination of their trapping mechanisms

M. Gerardin, E. Gilabert, D. Horlait, M.F. Barthe, G. Carlot

▶ **To cite this version:**

M. Gerardin, E. Gilabert, D. Horlait, M.F. Barthe, G. Carlot. Experimental study of the diffusion of Xe and Kr implanted at low concentrations in UO2 and determination of their trapping mechanisms. Journal of Nuclear Materials, 2021, 556, pp.153174. 10.1016/j.jnucmat.2021.153174 . hal-03414557

HAL Id: hal-03414557
https://hal.science/hal-03414557

Submitted on 5 Nov 2021

HAL is a multi-disciplinary open access archive for the deposit and dissemination of scientific research documents, whether they are published or not. The documents may come from teaching and research institutions in France or abroad, or from public or private research centers.

L'archive ouverte pluridisciplinaire **HAL**, est destinée au dépôt et à la diffusion de documents scientifiques de niveau recherche, publiés ou non, émanant des établissements d'enseignement et de recherche français ou étrangers, des laboratoires publics ou privés.

Experimental study of the diffusion of Xe and Kr implanted at low concentrations in UO_2 and determination of their trapping mechanisms

M. Gérardin[1,2*], E. Gilabert[3], D. Horlait[3], M-F. Barthe[4], G. Carlot[1]

[1] *CEA, DEN, DEC, F-13108 Saint Paul lez Durance Cedex, France*
[2] *Université de Lorraine, GeoRessources, CNRS, F54000 Nancy, France*
[3] *Université de Bordeaux, CNRS, CENBG-IN2P3, F-33170 Gradignan, France*
[4] *CEMHTI/CNRS, Université d'Orléans, 3A rue de La Férollerie, 45071 Orléans CEDEX 2, France*

* *Corresponding Author : marie.gerardin@univ-lorraine.fr*

Abstract

The fission of uranium dioxide produces gaseous elements degrading nuclear fuel properties. A thorough understanding of the transport and release of gaseous products is thus essential. The present work focuses on xenon and krypton migration mechanism in uranium dioxide. Desorption experiments on ion implanted UO_2 were performed at 1300°C. Xe and Kr releases were simulated using a mesoscale model that was developed taking into account single gas atom diffusion and defect traps. We showed that the defects have a high influence on Xe and Kr migration mechanisms and therefore have to be considered to accurately determine diffusion coefficients. We evaluated the diffusion coefficient of Xe and Kr at $(1.73 \pm 0.15)\text{x}10^{-20}$ m^2/s at 1300°C and we showed that the diffusion of rare gases is subjected to two trapping mechanisms. The first occurs during the ion implantation and the second during high-temperature annealings. The nature of the trapping sites is discussed in the light of the literature on radiation induced defects. This study also consolidates the use of non activated UO_2 implanted with heavy ions as a less-hazardeous substitute for irradiated UO_2.

Keywords

Uranium dioxide – Rare gases – Diffusion – Modelling – Ion implantation – Radiation induced defects

Highlights

- Diffusion of Xe and Kr implanted UO_2 was studied at 1300°C
- A diffusion model based on Fick's second law was developed
- Xe and Kr diffusion coefficient at 1300°C was found to be $(1.73 \pm 0.15)\text{x}10^{-20}$ m^2/s
- Xe and Kr migration is subjected to two trapping mechanisms due to radiation induced defects

1 Introduction

The behavior of fission products in uranium dioxide has been widely studied over the years by experimental and theoretical approaches. Significant quantities of rare gases are produced during fission of uranium and plutonium isotopes (roughly 0.31 atoms of Xe and Kr for one fission reaction [1], [2]). During irradiation, a fraction of the gaseous fission products is released into the free volume of the fuel pin, increasing the pressure inside the cladding. Gas release degrades the thermal conductivity of the fuel pin and the retention of gaseous elements in the fuel induce swelling due to gas bubble formation. To prevent cladding failure and to increase the fuel performance, the behavior of fission gases in irradiated UO_2 needs to be better predicted [3].

The current knowledge of rare gas diffusion in UO_2 is described in the exhaustive reviews of Matzke [4] and Rest et al. [5]. Experimental data on fission gas migration highlight three separate linear regimes in the Arrhenius plot of the Xe diffusion [6], currently used to simulate gas release in the fuel performance code [5]. In the thermal diffusion domain (T>1200°C), the diffusion coefficient of Xe and Kr decreases with the burn-up [7]–[9] as illustrated in Fig. 1. The diffusion coefficient also depends on the stoichiometry [10]–[13]. Most notably, Miekeley and Felix [10] reported that in $UO_{2\pm x}$, the diffusion coefficient increases for x over 2.021 and decreases for x below 1.997.

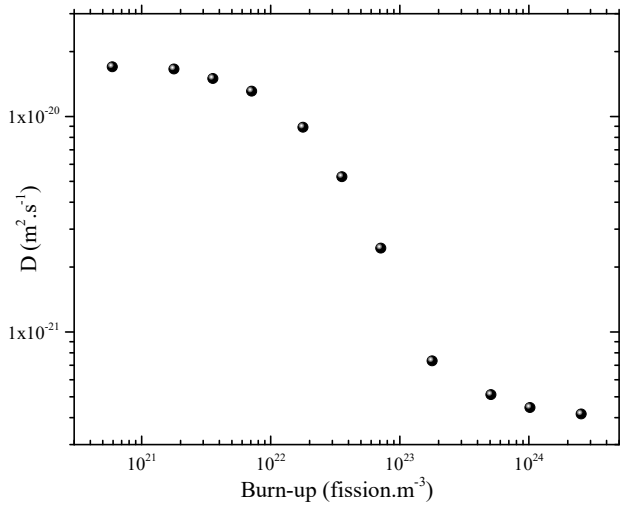

Fig. 1 – Diffusion coefficient measured at 1200°C (thermal diffusion regime) as a function of irradiation exposure in stoichiometric UO_2. Reproduced from [8]

The decrease in apparent diffusivity of xenon with increasing dose is explained on the assumption that beyond 10^{22} fission.m^{-3}, pre-existing pores and radiation-induced defects act like trapping centers [4], [7]. Some gas atoms interact with these traps and become immobile. The apparent diffusivity is then drastically reduced.

In most cases, diffusion coefficients were obtained from release experiments using Booth's sphere model [14]. This pioneer model simulates the microstructure by a set of equivalent spheres that are independent of each other. Release occurs by gas diffusion to the surface of these spheres. The model only requires the evaluation of the radius of the hypothetical sphere. However, the assumption that equivalent spheres represent the microstructure can be misleading [15]. Also, the burst release, described as a high release occurring at the beginning of the annealing, is not considered in Booth's model though it happens to comprise more than half of the total gas release [4]. According to literature, the burst release could be a surface effect [8], [16], thermally activated [16]–[19], that depends on grain boundaries [12], porosity [19] and stoichiometry [16], [20]–[22]. According to XRD measurements and recent in-situ TEM observations on implanted or irradiated UO_2 during annealing [23], [24], we might

add that the thermal recovery of point and extended defects could also influence the burst release. Considering Weber's work [23] on lattice defects in alpha-irradiated UO_2, thermal recoveries of point defects are observed mainly during the first 5 minutes annealing. Also, Onofri et al. [24] showed by in situ TEM observations that populations of dislocation loops and lines induced by heavy ions implantation in UO_2 change only within the first minutes of annealing. Based on these observations and on the assumption that gas atoms could interact with those defects, the amplitude and duration of the release by burst might also depend on the thermal recovery of point and extended defects. The burst mechanism is still a subject of active discussion since it depends on a large number of co-dependent experimental parameters. Its understanding requires an extensive experimental study on the defects population and their thermal recovery depending on the surface, the grain boundaries, the porosity and the stoichiometry of the $UO_{2\pm x}$ samples.

The purpose of this work is to get further insight into the mechanisms of Xe and Kr diffusion in UO_2 and especially their retention due to radiation damages. The presence of Kr and Xe in UO_2 is reproduced using the ion implantation technique enabling to control gas and defect concentrations. Implantations at various fluences were performed on polycrystalline and monocrystalline samples followed by annealing experiments at 1300°C. This work is focused on the diffusion at 1300°C where the thermal diffusion is dominating over the diffusion assisted by radiation damages [6]. To determine diffusion coefficients from experimental release rates, we developed a diffusion model combining well-known diffusion parameters: the burst effect, the trapping by radiation induced defects and the diffusion via Fick's second law.

2 Experimental

UO_2 polycrystalline samples are obtained from unirradiated fuel pellets (diameter of 8 mm) fabricated at CEA Cadarache [25]. Pellets are cut in discs, polished down to ~500 µm thickness and annealed at 1700°C during 24 hours under a reducing atmosphere (Ar-5%H_2). A second polishing treatment with a colloidal silica suspension (OP-U by *Struers* [26], [27]) is performed to eliminate the grain boundaries grooves [28]. Grain size on those samples is evaluated at 7.6 µm (± 1.5 µm uncertainty). In order to evaluate the influence of grain boundaries, monocrystalline samples were also studied. These samples were obtained by crystal growth during a slow cooling from a liquid phase [29]. Fragments (~ 5 x 5 mm) of the as-obtained monocrystalline block were polished and annealed at 1700°C during 24 hours under Ar-5%H_2. A thermodynamic calculation based on TAF-ID (Thermodynamics of Advanced Fuels – International Database) [30] outputs samples with stoichiometry (O/U) ranging from 1.9996 to 1.9998. Note that the gap to stoichiometry is too small to have a significant influence on the diffusion considering the work of Miekeley and Felix [10]. In order to study the effect of preparation conditions on gas diffusion, one monocrystalline sample was polished with OP-U solution after the first annealing at 1700°C. Also, some polycrystalline samples were treated with a second annealing at 1400°C during 4h under Ar-5%H_2 (after the first annealing at 1700°C and the OP-U polishing) to remove possible polishing defects, which could influence gas diffusion near the surface. Samples preparation characteristics are given in Table 1.

Sample Type	Preparation cond.	U/O	Ion	Implantation fluence (i/cm^2)	Name
Monocrystalline	A1	1.9996	800 keV Xe	(1.2±0.1).10^{11}	Xe11m-1a
	A1 OP-U			(9.5±1.0).10^{10}	Xe11m-1b
	A1			(6.0±0.6).10^{12}	Xe12m
	A1			(5.0±0.5).10^{13}	Xe13m
	A1			(5.0±0.5).10^{14}	Xe14m
	A1	1.9996	500 keV Kr	(2.0±0.2).10^{12}	Kr12m
Polycrystalline	A1 OP-U	1.9996	800 keV Xe	(1.2±0.1).10^{11}	Xe11p-1a
	A1 OP-U A2	1.9998		(1.4±0.1).10^{11}	Xe11p-1b
	A1 OP-U			(6.0±0.6).10^{12}	Xe12p
	A1 OP-U	1.9996		(1.2±0.1).10^{13}	Xe13p-1
	A1 OP-U			(5.0±0.5).10^{13}	Xe13p-2
	A1 OP-U A2	1.9998	500 keV Kr	(1.5±0.2).10^{11}	Kr11p
	A1 OP-U A2			(2.0±0.2).10^{12}	Kr12p

Table 1 – Samples preparation and implantations conditions

A1: Annealing at 1700°C during 24 hours under Ar-5%H$_2$
OP-U: Polishing treatment following A1
A2: Second annealing at 1400°C during 4 hours under Ar-5%H$_2$ performed after OP-U.

Samples were implanted at room temperature with 800 keV ^{129}Xe or 500 keV ^{83}Kr at fluences ranging from 9.5x10^{10} to 5x10^{14} i/cm^2. This wide range comprising such low fluences was achieved using the implantor IMIO400 at IP2I (Institut de Physique des 2 Infinis de Lyon - France). To verify the fluence, 4 Al foils were placed aside the UO_2 samples during ion implantations on each sample holder. The fluence was determined using TDS (described below) by melting the Al foils. The fluence of each sample was fixed to the mean value found on each sample holder and the fluctuation was evaluated at 10%.

The SRIM simulation code [31] was used to calculate the profiles of gas content and atomic displacements (dpa). The threshold displacement energies for oxygen and uranium were set to 20 and 40 eV respectively [32], [33]. According to SRIM calculations (Quick calculation damage), xenon or krypton projected range is 148 nm where the gas concentration reaches a maximum of about 0.08 ppm at 1x10^{11} i/cm^2. The damage area is created on the first 250 nm from the surface, with a maximum at ~75 nm depth (Fig. 2).

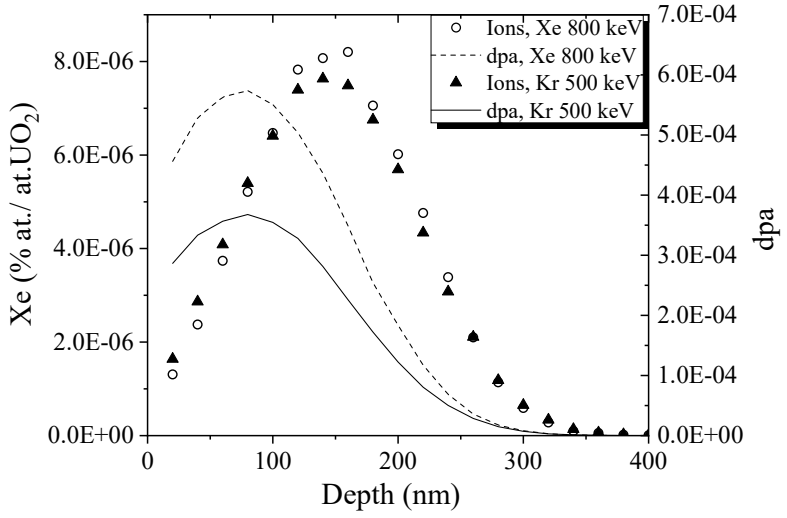

Fig. 2 - Depth profiles of 800 keV xenon or 500 keV krypton implanted with a fluence of 10^{11} i/cm^2 in UO_2. Gas content and damage profile given by SRIM [31]

Desorption experiments at a constant temperature were performed on the PIAGARA platform at the CENBG (Centre d'Etudes Nucléaires de Bordeaux-Gradignan). The high vacuum (down to few 10^{-9}

mbar) achieved by the device allows for measurements of very low amount of gases released from uranium dioxide [34], [35]. More details about the setup can be found in these references [36], [37]. This experimental device is made of (1) the heating chamber comprising the sample placed in a platinum crucible and a set of valves and various calibrated volumes that allow to take gas samplings, (2) several chemical traps (for the purification of gas samplings), (3) the calibration setup: a ^{82}Kr or ^{129}Xe calibrated monoisotopic reference gas with a specific precisely known concentration and (4) the mass spectrometer measuring the isotopic ratio between Kr or Xe released from the sample and from the reference gas addition.

The sample is placed into the cold part (upper part) of the heating chamber. As the lower part of the heating chamber reaches the required temperature, the sample is pushed down in the hot crucible. Hence the sample reaches the required temperature in a matter of seconds. Since the first gas extraction and analyze is made after 10 minutes, the effect of temperature rise of the sample on gas release is considered negligible. Then, samplings and analyses are made down to every 20 minutes (minimum time span required to expand gas samplings, to do the measurements in the mass spectrometer and evacuate analyzed gas by pumping in-between measurements). Release curves are constructed from the cumulated gas releases.

Note that the uncertainty on individual points obtained by TDS is mostly related to mass spectrometry measurements. The error on the fluence cannot be included on gas release curves because it is not related to each point taken individually. The fluence uncertainty is introduced for data treatment.

3 Results

Release rates at 1300°C of 800 keV Xe or 500 keV Kr implanted in UO_2 samples are plotted in Fig. 3 (for low fluences) and in Fig. 4 (for higher fluences). Please refer to Table 1 for more details on surface treatments applied to samples.

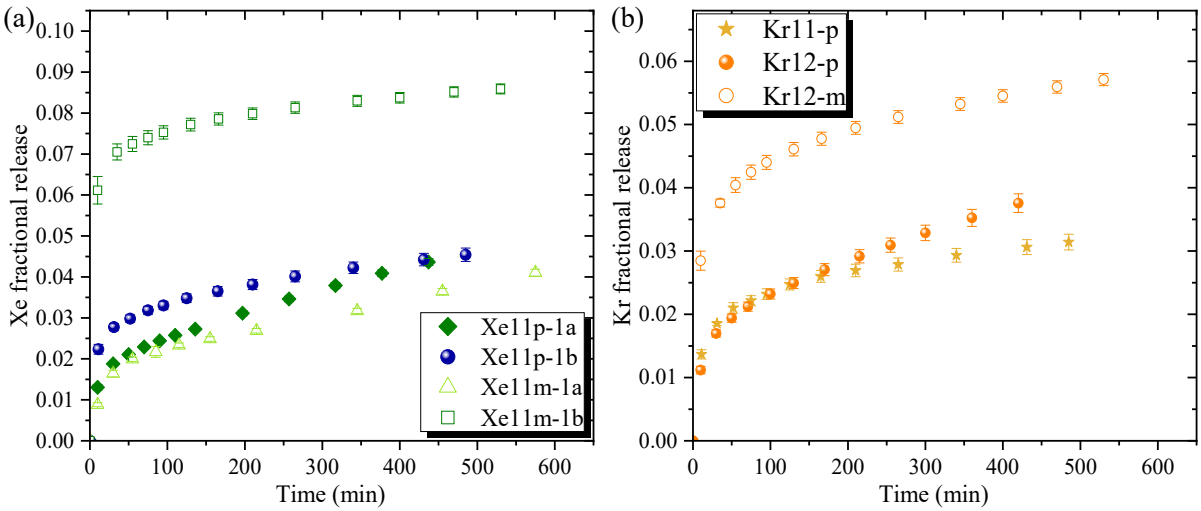

Fig. 3 – Cumulated release fractions of (a) 800 keV Xe and (b) 500 keV Kr from low fluence samples (≤ $2x10^{12}$ i/cm²) (1300°C annealings).

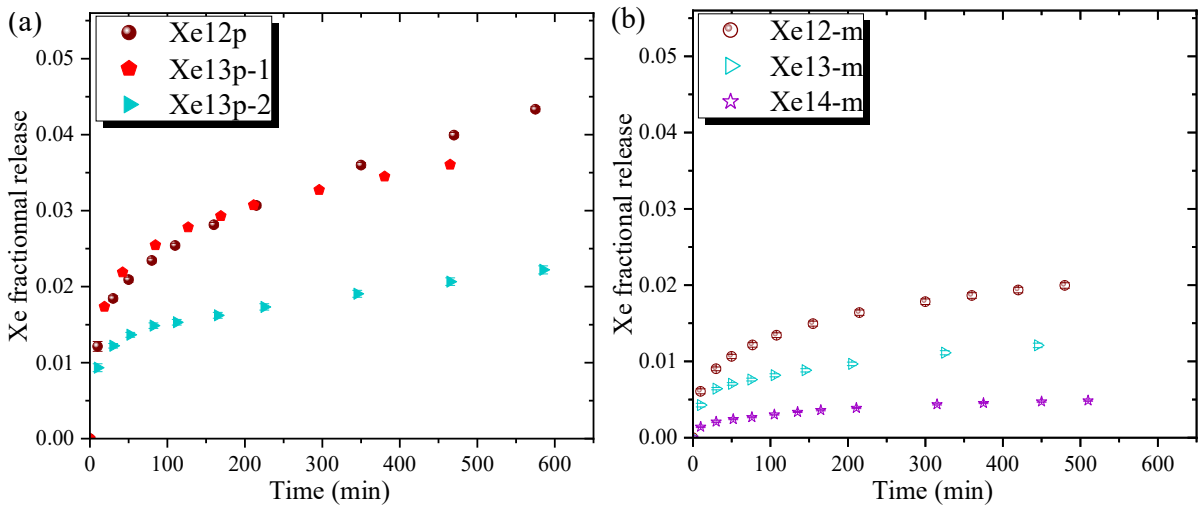

Fig. 4 – Cumulated release fractions of 800 keV Xe implanted at fluences ranging from $6x10^{12}$ to $5x10^{14}$ i/cm² in (a) poly-crystalline or (b) monocrystalline UO_2 samples (1300°C annealings).

The isotherms exhibit a high release dominant during the first few tens of minutes, typical of the burst effect [8], [12], [16]–[22]. After the release by burst, the release rates display a diffusional process. The gas release during the diffusional process decrease with increasing fluence (Fig. 4). This trend is independent of the sample structure (mono- *vs.* poly-crystalline).

4 Gas release modelling

4.1 Presentation of the employed model

In order to simulate gas release from isotherms obtained by thermal desorption, we developed a diffusion model based on the Fick's second law. The model (see schematic representation in Fig. 5) includes 4 main mechanisms:

The burst release, which was not considered in previous models to our knowledge. In our experiments, the burst release usually accounts for about half of the total gas release, motivating that this release should be taken into account. The physical properties of the burst release being not well-defined implies a delicate choice on its modeling. Multiple ways to implement the burst release in the diffusion model are discussed in Appendix A. We determined that the most reasonable model so far is to consider this process as an equilibrium state mechanism at the beginning of the annealing. We will thereby consider a fraction of the mobile gas that reaches a lattice site enabling its instant release to the surface. We could consider that this fraction diffuses with a coefficient D_2, different from the one on the diffusion D (see paragraph below) but first tests show that this coefficient is so high compared to the diffusion D (4 orders of magnitude) that the burst can be approximated as an instantaneous release. The burst release B(t) is defined by a frequency ν_b (s^{-1}) and a characteristic duration τ (s) according to the following relation:

$$B(t) = \nu_b \times e^{-t/\tau} \quad (1)$$

The burst is considered negligible after a duration of 5τ.

The apparent diffusion. Given that we cannot argue that the diffusion coefficient found in the present study involve only one diffusion mechanism and the less energetic one, it is more reasonable to define the diffusion as apparent instead of intrinsic. Mobile gas atoms diffuse with a coefficient D (m^2/s) according to Fick's second law.

The trapping along the gas diffusion path, theoretically and experimentally described by [8], [20], [38]–[44]. Gas atoms originally mobile could get trapped along their diffusion course by radiation induced defects. The present model considers that mobile gas atoms are trapped with the frequency $A(x)$. The trapping rate is based on the assumption that it is diffusion-driven. It does not depend on annealing time but has a depth (x) dependence. We suppose that trapping occurs only in the damaged zone (Fig. 2). Its equation is defined as

$$A(x) = \nu_t \times DPn(x) \tag{2}$$

where ν_t is the trapping rate in s^{-1} and is considered constant: neither coalescence nor re-solution are taken into account (see Appendix A part (3) for discussion on the re-solution process). $DPn(x)$ is the normalized damage profile from SRIM calculations (Fig. 2). For the sake of our calculations, we assumed that $DPn(x)$ remains constant during the TDS treatments. This necessary choice is supported by the lack, to our knowledge, of publications reporting thermal defects change on low fluence implanted sample (< 10^{15} i/cm^2 [45], [46]). This assumption is discussed in Appendix B where the depth distribution of xenon after TDS treatment is presented. ν_t is usually defined as follows:

$$\nu_t = 4\pi . r_t . C_t(x,t) . D \tag{3}$$

where $C_t(x,t)$ is the trapped gas concentration and r_t (m) is the trap equivalent radius.

The trapping effect in highly irradiated UO_2, observed by [7]–[9] (see Fig. 1) and considered as the trapping of some of the gas atoms during irradiation or in our case, during ion implantation process. This effect is considered in our model as Fr_{init}, a fraction of gas trapped before the annealing at 1300°C.

Combining all models, the diffusion equations used in this model sum up as follows:

$$\begin{aligned} \frac{\partial C_m(x,t)}{\partial t} &= -B(t) \times C_m(x,t) + \frac{\partial}{\partial x}\left(D \frac{\partial C_m(x,t)}{\partial x} \right) - A(x) \times C_m(x,t) \\ \frac{\partial C_t(x,t)}{\partial t} &= A(x) \times C_m(x,t) \end{aligned} \tag{4}$$

Where $C_m(x,t)$ (m^{-3}) is the mobile gas concentration in the sample at a depth x and a time t, and $C_t(x,t)$ (m^{-3}) is the trapped gas concentration.

Special attention has been given to the value of the fraction of gas trapped along the diffusion path over the mobile gas. This fraction is defined as $T(t)$ and is calculated as follows:

$$T(t) = \frac{\int_{x=0}^{\infty} [C_t(x,t) - C_t(x,0)] dx}{\int_{x=0}^{\infty} C_m(x,0)\, dx} \tag{5}$$

The initial conditions (at t = 0) are:

$$\begin{aligned} C_m(x,0) &= (1 - Fr_{init}) \times C_{SRIM}(x) \\ C_t(x,0) &= Fr_{init} \times C_{SRIM}(x) \end{aligned} \tag{6}$$

Where $C_{SRIM}(x)$ (m^{-3}) is the gas content profile given by the SRIM simulations (Fig. 2).

The boundaries equations are:

$$\begin{aligned} &C_m(0,t) = 0 \\ &C_m(x,t) = 0\,, \qquad for\ x \geq 10\ \mu m \\ &C_t(0,t) = 0 \\ &C_t(x,t) = 0\,, \qquad for\ x \geq 10\ \mu m \end{aligned} \tag{7}$$

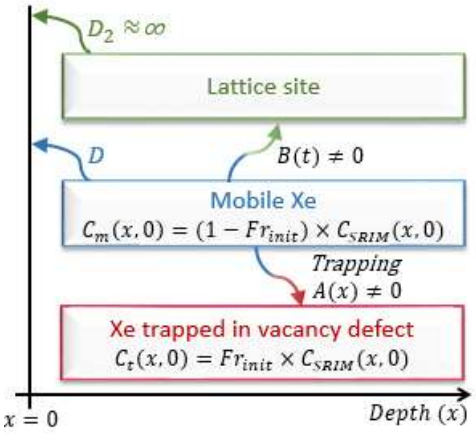

Fig. 5 – Modeling scheme of Xe (identically applicable to Kr) migration implanted in UO_2 considering the burst release with B(t), the diffusion D, the trapping along the gas diffusion path with A(x) and the initial trapping with Fr_{init}.

The gas release content is then evaluated as the difference between the initial gas content profile and the sum of mobile and trapped gas content profiles (see Appendix B for examples on gas content profiles after TDS treatment). The released fraction described as follows is calculated as the ratio between the gas release content and the initial gas content:

$$f_{sim}(t) = 1 - \frac{(\int_{x=0}^{x_\infty}[C_m(x,t) + C_t(x,t)])}{\int_{x=0}^{x_\infty} C_{SRIM}(x)dx} \tag{8}$$

Solving equations (1-5) was done by finite element calculation with FLEXpde™ software (PDE Solutions, Inc.). The iteration loop used to fit the experimental data was home developed based on LMFIT library on Python. Output parameters are D, ν_t, ν_b, τ and Fr_{init}. We determine that the dominant source of error for these output parameters comes from the uncertainty on obtained ion implantation fluences (±10%). One way to include the fluence fluctuation of 10% on the fit parameters errors is to evaluate the maximum variation of the parameters by fixing the fluence to the highest and lowest values. Therefore, three calculations were made for each sample: one at the fluence F, the second at the fluence $F + 0.1F$ and the third at the fluence $F - 0.1F$. These 3 calculations give the maximum variation of the diffusion coefficient, reported directly in Table 3.

The justifications of considering two trapping mechanisms to better describe Xe and Kr diffusion in UO_2 are provided in the following paragraphs, first for the trapping mechanism along the gas diffusion path and then for the trapping during ion implantation.

4.2 Trapping mechanism along gas diffusion path

To clearly observe the effect of considering a trapping mechanism along Xe or Kr diffusion on release rate, we will deliberately omit for now the trapping occurring during the implantation process, hence Fr_{init} parameter is set to 0. Two examples of experimental data simulations are shown on Fig. 6. The two examples concern annealing experiment at 1300°C from samples "Xe11p-1b" and "Kr12p" (see description in Table 1). First of all, isotherms are fitted with the burst release only (via ν_b and τ parameters), meaning that we did not consider any diffusion nor trapping frequency (**S1**) (see Fig. 6). We clearly see that the model distinguishes correctly the burst release from the diffusional regime. A

second simulation takes into account the burst and the diffusion coefficient D (**S2**) and a third one includes the burst, the diffusion coefficient and the trapping frequency ν_t (**S3**) (see Fig. 6).

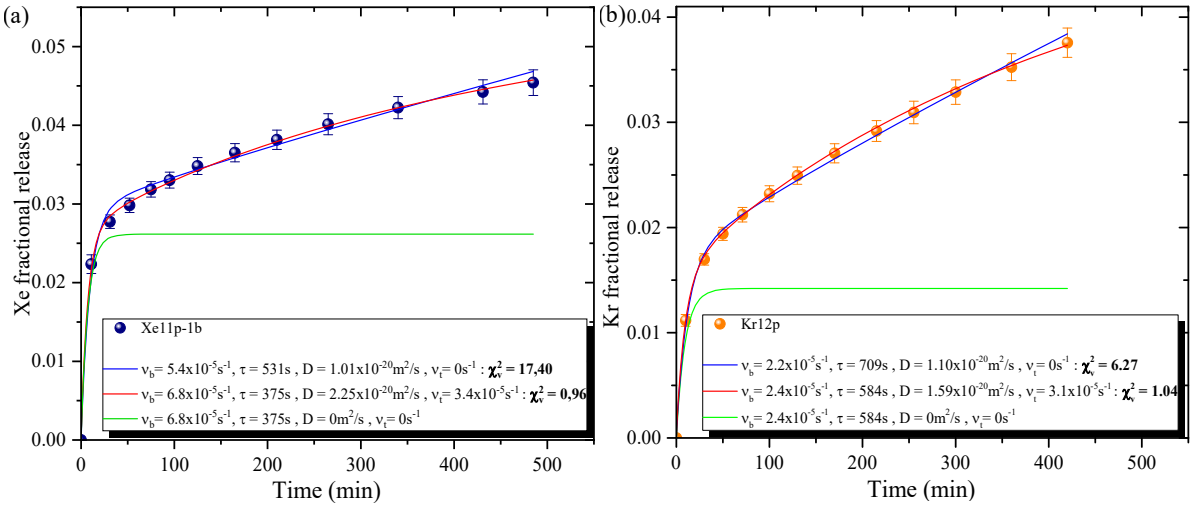

Fig. 6 – Simulations of fractional release at 1300°C from (a) "Xe11p-1b" and (b) "Kr12p" samples.

The "reduced chi square" value, $\chi_\nu{}^2$ is calculated by the model for the simulation **S2** and **S3**. For both samples, $\chi_\nu{}^2$ is clearly smaller in the case of **S3** meaning that the simulation is closer to the experimental data than **S2** (Table 2). This result suggests that the simulation of experimental isotherms is more representative when the trapping frequency is taken into account. Also, we observe that the non-consideration of the trapping frequency (**S2**) leads to an underestimation of the diffusion coefficient (Table 2).

Sample	Simulation	ν_b ($\times 10^{-5}\ s^{-1}$)	τ (s)	D ($\times 10^{-20}\ m^2.s^{-1}$)	ν_t ($\times 10^{-5}\ s^{-1}$)	$T(400)$ (%)	$\chi_\nu{}^2$
Xe11p-1b	**S2**	5.4 ± 0.6	531 ± 61	1.01 ± 0.05	0	0	17.40
	S3	6.8 ± 1.1	375 ± 71	2.25 ± 0.66	5.9 ± 1.4	50	0.96
Kr12p	**S2**	2.2 ± 0.2	709 ± 74	1.10 ± 0.05	0	0	6.27
	S3	2.4 ± 0.3	584 ± 85	1.59 ± 0.43	3.1 ± 1.3	34	1.04

Table 2 – Simulation parameters with or without a trapping rate ν_t (s^{-1}) used to fit "Xe11p-1b" and "Kr12p" experimental isotherms (Fr_{init} set to 0).

Table 2 reports the values of the trapped gas content after a 400 minutes annealing, $T(400)$, calculated from eq.5. For these cases (ν_t~ 3.1 for Kr and 5.9x10^{-5} s^{-1} for Xe), the trapped gas content at 400 min 1300°C annealing amounts to 34 and 50% of the mobile gas (i.e. of the implanted gas in this case since $Fr_{init} = 0$ for these implantation at low fluences, see part 4.3). Those high values indicate that the trapping mechanism along the gas diffusion path has a large impact on the gas behavior during annealing. This statement supports that this trapping mechanism cannot be neglected when studying heavy rare gases diffusion in uranium dioxide.

4.3 Trapping mechanism during ion implantation

To justify the existence of a trapping mechanism occurring at the ion implantation stage, we will first discuss simulation results when the initial fraction of gas trapped is not considered ($Fr_{init} = 0$).

The parameters of fit obtained by simulating each experimental isotherm (see Fig. 3 and Fig. 4) with $Fr_{init} = 0$ are presented in Table 3. The obtained diffusion coefficients are plotted in Fig. 7.

For all samples except for "Xe11m-1a", the values of the burst characteristic duration (τ) remain within the same order of magnitude with a median value at around 490 seconds, meaning that the burst duration is very close from a sample to another. The value of the burst release frequency characteristic ν_b however shows clear variations between samples, ranging from 0.4 and 26.2×10^{-5} s^{-1} and this variation is not correlated to sample preparation. According to literature, burst release is the consequence of various mechanisms occurring at the beginning of the annealing. Since it could be a surface effect, and/or depend on porosity, on stoichiometry, etc. (see Section 1), the discussion on ν_b variations requires more data from surface and bulk conditions that we are not able to provide. To bring insights on the burst mechanism, an extensive study should be engaged on gas release from samples, with surface and bulk conditions more rigorously controlled. In this paper, the burst release parameters will not be discussed any further. Note that the debatable identification of the burst mechanism does not discredit the discussion on the diffusion and trappings since the model clearly distinguishes the burst from the diffusional and trapping processes (see Fig. 6, fit S3 against S1).

Table 3 shows that the ν_t values (trapping rate along diffusion path) range from $<1 \times 10^{-5}$ to 9.1×10^{-5} s^{-1}. The variation of those values is relatively high and surprisingly do not appear to vary as a function of sample preparation, gas type, fluence nor samples microstructure (mono- *vs.* poly-crystalline).

On the apparent diffusion coefficient *D*, we first notice similar values for polycrystalline and monocrystalline samples. This was expected since the ion implantation depths are ~1 order of magnitude lower than the grain size in polycrystalline samples, hence very few of the released Xe or Kr would have reached a grain boundary on their path. Moreover, no significant differences were found on the apparent diffusion coefficients as a function of sample surface preparation. The OP-U polishing treatment or the second annealing at 1400°C have then no clear influence on the apparent diffusion. Also, it is notable to observe that at 1300°C, Xe and Kr diffuses in UO_2 with similar kinetics, considering the model sensitivity. Finally, it is clearly demonstrated by Fig. 7 that the apparent diffusion coefficients decrease with the implantation fluence from above 1.2×10^{13} i/cm^2.

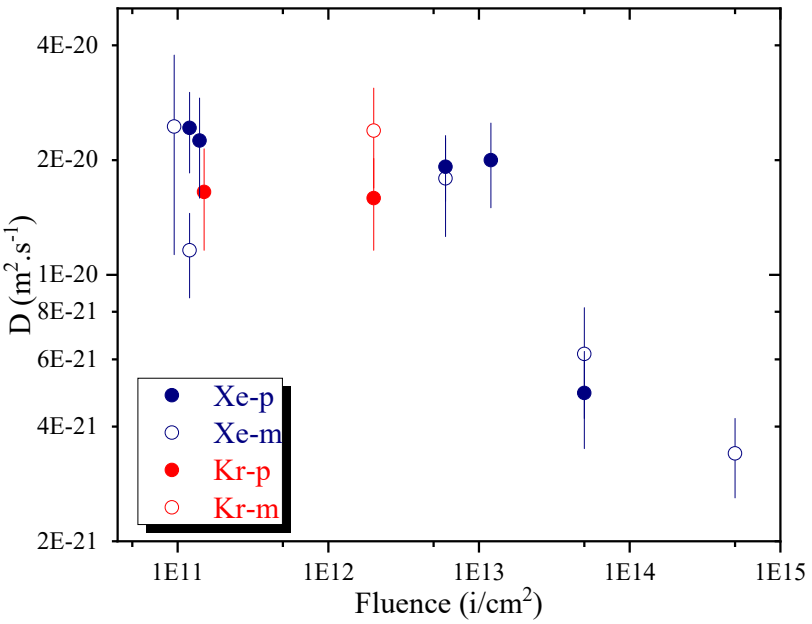

Fig. 7 – Xenon or krypton diffusion coefficient changes with the implantation fluence. Hollow symbols refers to monocrystalline samples and filled symbols to polycrystalline ones.

Up to 10^{13} i/cm^2, the apparent diffusion coefficient does not depend on fluence (nor ion type). We can then calculate the mean value (weighted by individual errors of diffusion coefficients) in the fluence range of 9.5×10^{10} to 1.2×10^{13} i/cm^2, which amounts to $(1.73 \pm 0.15) \times 10^{-20}$ $m^2.s^{-1}$.

The apparent diffusion coefficient change with the dose is consistent with previous results on xenon diffusion from irradiated UO_2 samples [7]–[9] (Fig. 1), where the diffusion coefficient tends to decrease with fission rate and thereby with defects content. In the case of [8], the diffusion coefficient decreases from approximately 10^{22} fission.m^{-3}. As a first and simplistic approximation, we can consider that gas and defects distribution are homogeneous in neutron irradiated samples and that one uranium displacement produces one defect. Considering the fission reaction energy of 200 MeV and the uranium displacement energy of 40 eV, a 10^{22} fission.m^{-3} irradiation corresponds to ~0.02 dpa. Our results show that a trapping mechanism also occurs in implanted UO_2 samples and is seen to have a quantifiable effect at fluences from around 1.2x10^{13} i/cm^2. This fluence corresponds to a radiation induced damage of about 0.07 dpa at the maximum (and 0.03 dpa at the mean value). Note that the comparison of gas and defects distribution between neutron irradiated and implanted samples is tricky. In implanted samples, gas and defects are heterogeneously distributed along the depth x (Fig. 2) and we could either consider as relevant a mean or a maximum value. Also, those values are taken from SRIM simulations that approximates the gas and defects distribution after implantation. Nonetheless the threshold dpa in our study and in Kaimal's [8] are interestingly close in spite of different experimental and calculation conditions.

We propose that the decrease of the apparent diffusion coefficient with the fluence is due to the trapping of a fraction of gas during the implantation process modeled by the Fr_{init} parameter. To determine the variation of the initial gas trapped concentration with fluence, release rates from samples implanted at a fluence greater than 1.2x10^{13} i/cm^2 are now simulated with $Fr_{init} \neq 0$. But as a new parameter is added, the simulation can no longer provide reasonable values of each 5 parameters (D, ν_b, τ, ν_t and Fr_{init}). For these simulations, we thus had to fix the value of D to the value calculated above for low fluences (1.73x10^{-20} m^2.s^{-1}). Simulation results are presented in italics in Table 3.

Name	Fluence (i/cm^2)	t_{final} (min)	ν_b ($\times 10^{-5}\ s^{-1}$)	τ (s)	D ($\times 10^{-20}\ m^2/s$)	ν_t ($\times 10^{-5}\ s^{-1}$)	Fr_{init} (%)
Xe11m-1b	(9.5±1.0).10^{10}	533	26.2 ± 4.9	285 ± 57	2.45 ± 1.32	7.2 ± 3.4	-
Xe11m-1a	(1.2±0.1).10^{11}	583	1.8 ± 0.1	1012 ± 107	1.16 ± 0.29	< 1	-
Xe11p-1a	(1.2±0.1).10^{11}	438	3.7 ± 0.5	478 ± 71	2.43 ± 0.58	2.0 ± 1.0	-
Xe11p-1b	(1.4±0.1).10^{11}	487	6.8 ± 1.1	375 ± 71	2.25 ± 0.66	5.9 ± 1.4	-
Kr11p	(1.5±0.2).10^{11}	487	3.2 ± 0.4	501 ± 87	1.65 ± 0.49	8.8 ± 1.7	-
Kr12m	(2.0±0.2).10^{12}	533	8.2 ± 1.1	393 ± 61	2.39 ± 0.70	7.8 ± 1.6	-
Kr12p	(2.0±0.2).10^{12}	422	2.4 ± 0.3	584 ± 85	1.59 ± 0.43	3.1 ± 1.3	-
Xe12m	(6.0±0.6).10^{12}	480	1.4 ± 0.2	465 ± 95	1.79 ± 0.53	9.1 ± 1.9	-
Xe12p	(6.0±0.6).10^{12}	583	2.6 ± 0.2	654 ± 68	1.92 ± 0.36	2.8 ± 0.4	-
Xe13p-1	(1.2±0.1).10^{13}	407	2.7 ± 0.2	693 ± 74	2.00 ± 0.50	7.2 ± 1.2	-
Xe13m	(5.0±0.5).10^{13}	445	1.3 ± 0.1 *3.1 ± 0.5*	530 ± 76 *535 ± 77*	0.62 ± 0.20 *1.73 (fixed)*	4.0 ± 1.8 *4.0 ± 1.7*	- *58 ± 10*
Xe13p-2	(5.0±0.5).10^{13}	600	1.9 ± 0.2 *5.7 ± 0.8*	486 ± 68 *491 ± 68*	0.49 ± 0.14 *1.73 (fixed)*	2.8 ± 1.1 *2.9 ± 1.0*	- *65 ± 7*
Xe14m	(5.0±0.5).10^{14}	513	0.4 ± 0.1 *1.5 ± 0.3*	361 ± 97 *379 ± 90*	0.34 ± 0.08 *1.73 (fixed)*	8.5 ± 1.0 *8.1 ± 0.9*	- *75 ± 3*

Table 3 – Simulation parameters from fractional releases at 1300°C of 800 keV xenon or 500 keV krypton implanted in UO_2 samples. For simulations with $Fr_{init} \neq 0$, D was set at 1.73x10^{-20} m^2.s^{-1}

For each release rate, the addition of the Fr_{init} parameter in the simulation has no influence on the τ parameter but tends to increase the ν_b values. This is easily explained because the mobile gas population available for burst release is smaller when $Fr_{init} \neq 0$ and to reach the same amount of gas released by burst, the ν_b value has to increase. On the other hand, the trapping frequency ν_t is not affected by adding Fr_{init}. It means that the trapping frequency is completely independent of the initial trapping and of xenon content. The fraction of trapped gas during implantation strongly increases with the fluence (Table 3). At 5x10^{14} i/cm^2, corresponding to a dpa at peak maximum of about 2.8, 75% of xenon is trapped at the beginning of the annealing.

5 Discussion

When applied to the gas release rate at 1300°C, the diffusion model developed for this work enables us to better describe gas diffusion mechanism like the trapping effects.

First, the apparent diffusion coefficient is determined at 1.73×10^{-20} m^2/s at 1300°C. Because of the varying experimental conditions, literature on xenon temperature dependence in irradiated UO_2 is wide. To compare the present result to literature, we will only consider studies performed on stoichiometric UO_2 sintered pellets irradiated at a burn-up lower than 10^{22} fission.m^{-3}. Under those conditions, the xenon diffusion coefficient amounts to 5.3×10^{-20} m^2/s at 1300°C [8], [47]. The present value of xenon and krypton is slightly lower than the one found in the literature but remain in the same order of magnitude. The main differences between the literature and our result is the model used to evaluate the coefficient. Kaimal et al. [8] and Barnes et al. [47] used the Booth's model [14]. It approximates the microstructure as a set of equivalent spheres and does not consider the burst release, nor the trapping of gas atoms along their diffusion path. Nonetheless, the diffusion model presented in this work being totally different from the Booth's model, the two diffusion coefficients are interestingly close.

During the implantation process at fluences over 1.2×10^{13} i/cm^2 (corresponding to ~0.07 dpa at the maximum of the defect profile induced by Xe 800 keV, see Fig. 2), a fraction of gas is trapped in the sample and this fraction increases with the fluence. Theoretical studies show that after ion implantation or irradiation, small vacancy clusters are likely to be formed in displacement cascades [48]–[51]. Also, it has been demonstrated that the density of each cluster decreases with their size [48], [52], meaning that di-vacancies concentration is higher than that of the bi-Schottky defect, which is higher than that of nanometer sized voids. Latest TEM observations agree with theoretical calculations since small voids are observed after ion implanted in UO_2 samples from 0.03 dpa approximately [53]. Their density increases sharply with the damage and up to 0.2-0.3 dpa, the density reaches a saturated state at around $0.6\text{-}3.10^{24}$ m^{-3}. The size of those voids remains constant with damage. Their diameter lies between 0.56 ± 0.11 nm and 1.05 ± 0.21 nm depending on TEM settings, which are of a major importance to precisely determine the actual void size [53]. Depending on void size observed by TEM, we could identify the presence of either small vacancy defects (diameter of about 0.56 ± 0.11 nm) or nanometer sized cavities. Either way, at around 0.07 dpa, the damage rate is sufficient to nucleates voids considering previous work [53]. Also, many studies employing density functional theory (DFT) [54]–[65] and molecular dynamics (MD) with empirical potentials [13], [66]–[69] have shown that the most favorable trap site of xenon or krypton is an uranium vacancy related defect. In most cases the trap site has also oxygen vacancies. It can thus be assumed that trapping mechanism occurring during the implantation process is related to small vacancy cluster such as di-vacancies or Schottky defects and to nanometer sized cavities. Note that in this work the fraction of gas trapped during the implantation process appears for a damage rate at around 0.07 dpa but below this value, small voids are already formed [53]. First we should mention that 0.07 dpa is the level of damage where the model is capable of detecting a change on the diffusion. A potential smaller change on the diffusion occurring at a lower damage level might not be revealed on account of the model sensitivity and uncertainties associated to desorption experiments. On the other hand, the size and nature of small voids formed at a dpa lower than 0.07 might slightly differ from those formed at 0.07 and higher dpa. Also the trapping probability of gas atoms is expected to differ from one defect to another. The traps responsible of the trapping mechanism during the implantation process might be formed only from 0.07 dpa approximately and since the fraction of trapped gas increases with the fluence, their concentration and/or their size increases with the fluence.

Besides, a trapping frequency (ν_t) is needed to simulate experimental data. This mechanism is defined as the trapping of gas atoms along their diffusion path by defects and is active for the whole range of fluences investigated in the present work. It has no fluence dependency at first sight suggesting that the

product $r_t.C_t$ (see eq.3) remain roughly constant in the damage dose investigated in our study from $5.5x10^{-4}$ dpa to 4.6 dpa. As indicated above, TEM studies on implanted samples have shown the formation of vacancy clusters for damage doses above 0.2-0.3 dpa. The lowest fluence in this study induces a maximum damage of $5.5x10^{-4}$ dpa. To our knowledge, no TEM investigation was performed on implanted samples with such a low damage. Displacement cascades induced by ion implantation should form smaller vacancy clusters. With temperature, XAS (X-ray Absorption Spectroscopy) characterizations reveal that xenon or krypton highly implanted in UO_2 (1 to 4 MeV Kr and 390 keV Xe implanted at fluences around 10^{15} and 10^{16} i/cm^2) are likely to aggregate to form pressurized clusters [70]–[72]. Also, experimental evidence of xenon presence in smaller defect after annealing at 1400°C was given by XAS characterization in samples implanted with 390 keV at the fluence of $1.7x10^{15}$cm^{-2} corresponding to a high damage dose of 55 dpa. [46]. The author suggests that besides bubbles nucleation, xenon is bound to the Schottky defect induced by ion implantation and does not seem to migrate with temperature (up to 1400°C). Note that XAS characterizations were performed on highly irradiated samples (from 10^{15} i/cm^2) and to our knowledge, no experiments on low fluences implanted samples were conducted. The trapping mechanism along gas diffusion path remains complex since the temperature dependence on vacancy clusters is not well described and also because the fluence might have an influence on those microstructure changes with temperature. At this point, we can assume that for low fluences samples, gas atoms are trapped in small vacancy related defects like the Schottky defect experimentally evidenced by Bès et al. [46]. For higher fluences implanted samples, in which larger defects like nanometer sized voids are expected to be formed by ion implantation, one might raise the possibility that the latter are also participating to the trapping of gas atoms along their diffusion path. Nonetheless, we showed that the trapping frequency has no dependency with the fraction of gas trapped during the implantation. If the trapping sites were the same, we should attest, just as for Fr_{init}, an increase of ν_t as the damage dose increases. Since the trapping frequency remains broadly constant with the damage dose, we can reasonably state that the gas trapped along its diffusion path involves defects of a different nature than those involved on the trapping during the implantation process.

6 Conclusion

The thermal diffusion at 1300°C of rare gases implanted in uranium dioxide has been investigated in the $9.5x10^{10}$ to $5x10^{14}$ i/cm^2 fluence range. The isothermal release rate of Xe and Kr was measured by thermal desorption at 1300°C. We developed a new diffusion model based on known mechanisms such as the release by burst, the trapping by radiation induced defects and the diffusion via Fick's second law to determine the diffusion coefficient of Xe and Kr in UO_2 and trapping parameters. Release rates showed a notable burst release and since its physical properties are not clearly understood, we discussed multiple ways to implement it in the diffusion model (see Appendix A). Whichever the burst modeling, we determined that Xe and Kr diffuse according to the same mechanisms at 1300°C with a same apparent diffusion coefficient of $(1.73 \pm 0.15)x10^{-20}$ m^2/s. Also, we demonstrated that a better determination of the diffusion implies the consideration of two significant trapping mechanisms. This result is in agreement with similar studies on rare gases diffusion in irradiated UO_2, approving that non active material implanted with Xe and Kr is a rather good substitute to study rare gases diffusion (and conveniently less hazardous and costly to work on). This statement could clearly facilitate further experimental work on rare gas diffusion and/or damage characterization.

One trapping mechanism occurs during the implantation process from a fluence between $1.2x10^{13}$ and $5x10^{13}$ i/cm^2 and the fraction of gas trapped increases with the fluence. This trapping mechanism is assumed to be related to small vacancy cluster such as di-vacancies or Schottky defects formed in displacement cascades and to a lesser extent, to nanometer sized voids. The second trapping mechanism occurs during the annealing experiment at 1300°C and is defined as the trapping of gas atoms along

their diffusion path by vacancy related defects. The nature of trapping sites remain complex since their thermal behavior is not fully understood. The present results tend to show that small vacancy clusters are trapping xenon (and krypton) atoms and that their nature and size differ from those involved on the trapping during the implantation process. An extensive study on the defects nature and proportion changes with the fluence and with the temperature is needed to bring new insights on the identification of the xenon and krypton trapping site(s) during implantation and along their diffusion paths.

Acknowledgments

This research is part of the INSPYRE project, which has received funding from the Euratom research and training program 2014-2018 under Grant Agreement No 754329. We sincerely thank Anthony Duranti (IP2I/IN2P3 CNRS) for performing Xe and Kr implantation. We also thank Claire Onofri (CEA/DEN) for uranium dioxide pellets fabrication and for fruitful discussions about radiation induced voids.

Appendix A

Depending on the physical phenomenon regulating the burst release, release rate modeling can be achieved in multiple ways. This appendix describes three other interesting models to simulate Xe and Kr experimental releases. Compared to the selected model presented in 4.1, these other models are no good candidates to accurately simulate our experiments but they give more insights on the burst modeling choices, and eventually allow ruling out some plausible diffusion and trapping processes.

(1) For the burst release modelling, instead of considering that a fraction of mobile gas reaches a lattice site, which allows for its instant release, we could assume that some gas atoms are already (after implantation) in the lattice site and that the temperature activates the quick release. In this case, an initial fraction of the mobile gas Fm_i is retained in a site and rapidly diffuses with the coefficient D_2 to the surface at the beginning of the annealing (see Fig. 8(1)). Surprisingly, no trapping frequency is needed to correctly fit the experimental data, which is in disagreement with previous studies on rare gases release rates [8], [20], [38]–[44]. This model might then not reflect accurately all of the phenomenon describing xenon diffusion. Nonetheless, initial trapping of gas atoms might be one (but not the sole) of the processes of the burst release.

Using this model, the apparent diffusion coefficient is of about 6.10^{-21} m^2/s, and from 2.10^{13} at/cm^2, the diffusion decreases as observed using the previous model. The diffusion coefficient D_2 is around 3.10^{-17} m^2/s and does not significantly change with the fluence, sample type nor preparation. Finally, the fraction of gas atoms trapped at the beginning of the annealing, Fm_i, gradually decreases from approximately 3% for the lowest fluence to 0.5% for the highest.

(2) The burst release seems to be subjected to surface effect [8], [16]. Another way to model the burst release is to define a depth dependent diffusion coefficient as follows: a high coefficient at the surface vicinity D_S and a lower diffusion in the volume D (see Fig. 8(2)). To try this model, we used a defined limit Xl (m) from the surface to separate the surface diffusion from the one in the volume[1], instead of using a gradient probably more realistic but too complex to implement considering the resolution of our release experiments (3 to 4 experimental points for the 60' burst). Also in this model, we could implement a trapping parameter at the surface different from the one in the volume. But the burst being short and for the sake of simplification, we chose not to consider any trapping parameter in the surface (Fig. 8(2)).

With this model, the diffusion coefficient in the volume is around 6.10^{-21} m^2/s, which is slightly lower than the one with the model presented in paragraph 4. From 2.10^{13} i/cm^2, the volume diffusion coefficient decreases with the dose, as already observed. The surface diffusion coefficient is two order of magnitude higher than the volume diffusion and no variation was found with the fluence, sample type, nor preparation. The trapping rate during annealing ν_t (s^{-1}), only defined in the volume remain in the same order of magnitude (0 to $8x10^{-5}$ s^{-1}) and we still did not observe any dependence with the fluence, sample type nor preparation.

(3) On a completely other basis, what we previously defined as a burst effect might also be described as a diffusional process subjected to a strong trapping along with a re-solution effect. According to [39], [73], gas enclosed can be dissolved by an irradiation induced re-solution process. So far, no physical phenomenon can explain a re-solution mechanism in implanted UO_2. In order to discuss the process of

[1] It is interesting to note that the modeling of the burst effect by a higher surface diffusion produces a depleted zone on the sample surface, between 0 and Xl.

diffusion combined to trapping and re-solution mechanism in implanted samples, simulations of the release rate are carried out using the equations:

$$\begin{aligned}\frac{\partial C_m(x,t)}{\partial t} &= \frac{\partial}{\partial x}\left(D\frac{\partial C_m(x,t)}{\partial x}\right) - A(x)\times C_m(x,t) + \nu_r \times C_t(x,t)\\ \frac{\partial C_t(x,t)}{\partial t} &= A(x)\times C_m(x,t) - \nu_r \times C_t(x,t)\end{aligned} \quad (9)$$

With ν_r (s^{-1}) is the re-solution frequency (see Fig. 8(3) for the modeling scheme). Few simulation attempts show that this model properly reproduces the first 50 minutes of the release rate but fail to represent the gas release at higher annealing time.

For guidance, this model calculates a gas diffusion coefficient of about 10^{-19} m^2/s. The trapping mechanism along the gas diffusion path is high to simulate the slope change of the gas release at around 50 minutes (ν_t amounts to ~75 s^{-1}). The re-solution process (ν_r ~3.6 s^{-1}) increases the gas release but the simulations do not fit the experimental release. Thus, this model consolidates the existence of a burst release at the beginning of the annealing, independent of the apparent diffusion[2] of rare gases in UO_2. Also, those simulations show that the re-solution effect is not a significant mechanism in implanted samples, as expected according to previous statement.

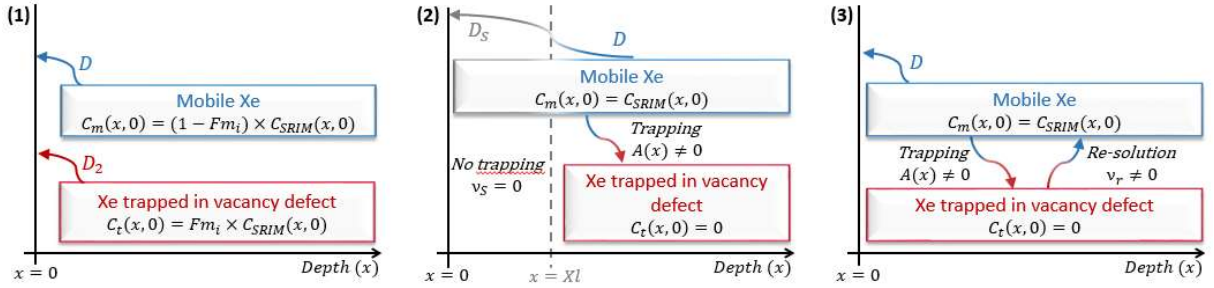

Fig. 8 – Schematic representation of the burst modeling by (1) a fraction of trapped gas at the beginning of the annealing, (2) a depth dependent diffusion and (3) a diffusion process subjected to a trapping/re-solution mechanism.

Regardless of the model we choose to simulate the burst release, we inevitably observe the decrease of the apparent diffusion coefficient of xenon with the fluence from approximately 1.2×10^{13} at/cm^2. It means that the trapping of gas atoms during implantation is independent of the burst release (and vice-versa). Only the value of the apparent diffusion coefficient change depending on the model but it is not drastically different from a model to another (around 6.10^{-21} m^2/s and 1.73×10^{-20} m^2/s). Modeling of the burst release remain a challenge, mostly because it probably depend on multiple co-dependent effects. This paper bring light to some of the parameter that could influence the burst: surface effect, initial trapping in thermally activated defects and/or gas diffusion towards those thermally activated defects. For now, we determined that the most reasonable burst modeling is an equilibrium state mechanism simulated by the instant release of a fraction of the mobile gas (see section 4.1). Further insights on the release by burst are needed to complete the modeling scheme.

Appendix B

The depth distribution of mobile and trapped gas are obtained by the resolution of equations (4). The profiles of two samples, Xe11p-1a and Xe14m, before and after the TDS treatment are presented in Fig. 9.

[2] It is interesting to note that if the burst release is not taken into account and the diffusion coefficient is determined on the first points of release rate, the latter might be vitiated by an error of more than one order of magnitude.

The xenon profile before annealing is the one given by the SRIM software (C_{SRIM} in Fig. 9). For sample Xe11p-1a, all gas atoms are mobile at t=0 ($C_{SRIM}=C_m(x,0)$ and $C_t(x,0)=0$). For sample Xe14m, 75% of xenon are trapped after the implantation (see Table 3), which is clearly the dominant trapping process. During the TDS treatment, the initially mobile gas (25% for sample Xe14m and 100% for Xe11p-1a) diffuses and the atoms reaching the surface are released, but some of them are trapped along the gas diffusion path, which depends on the damaged profile $DPn(x)$ (see eq. (2) and Fig. 2). The mobile and trapped profiles after the TDS treatment are represented by the dotted lines in Fig. 9.

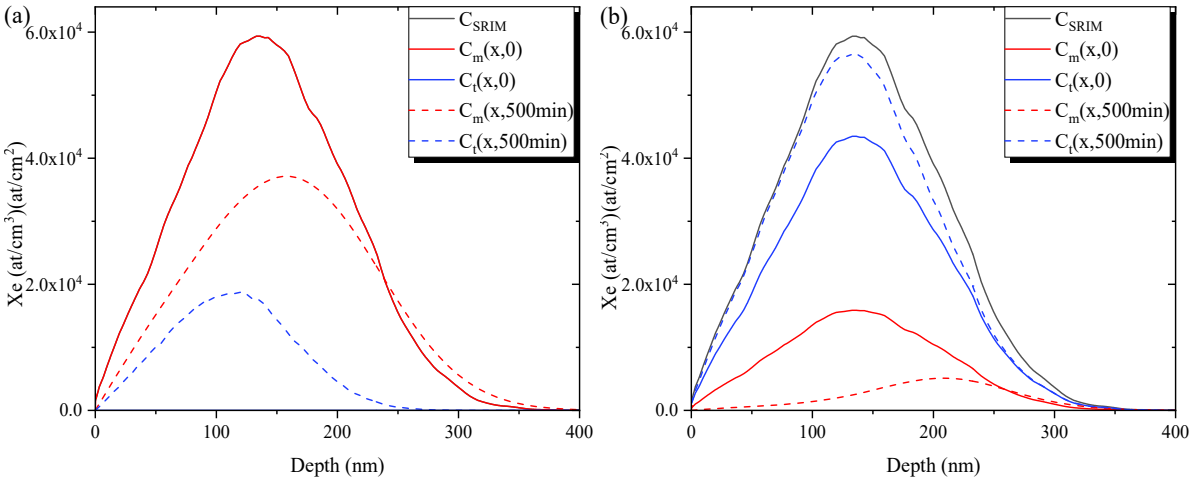

Fig. 9 – Changes on depth profiles of 800 keV xenon (normalized) during TDS treatment: (a) sample Xe11p-1a and (b) Xe14m. C_{SRIM} is the initial profile, Cm and Ct are respectively the mobile and trapped Xe components. Dotted curves are obtained from the fitting of the experimental results and correspond to the simulated profiles after 500 min of TDS annealing at 1300°C.

We assumed that $DPn(x)$ remains constant during the TDS treatment but the defects might actually evolve at 1300°C, leading to different trapping process. One way to include this behavior in the model is to define a trapping along the gas diffusion path that is time-dependent, $A(x,t)$ (see. eq. (2)). Nonetheless, no publication, to our knowledge, propose an equation simulating the time-dependency of the trapping along the gas diffusion path. Also, this new model would include one more parameter, impeding the reliability of the variable parameters considering the sensibility of our calculations. Finally, the time-dependency of the trapping probably depends on the fluence. At high implantation, larger defects like nano-void are formed and with temperature, they are likely to aggregate to form larger void. This behavior operates along with the probable annealing of other defects and the two process are in competition. One cannot simply evaluate the trapping dependency with the annealing time and with the fluence. Facing this issue, we considered $DPn(x)$ as constant because we assessed that it was the most reasonable choice.

References

[1] H. Bailly, D. Ménissier, et C. Prunier, *The Nuclear Fuel of Pressurized Water Reactors and Fast Reactors design and behaviour*, CEA, Eyrolles, Série synthèse. 1996.

[2] C. Ferry *et al.*, « Synthesis on the spent fuel long term evolution », CEA Saclay, CEA-R-6084, 2005.

[3] M. Tonks *et al.*, « Unit mechanisms of fission gas release: Current understanding and future needs », *J. Nucl. Mater.*, vol. 504, p. 300-317, juin 2018, doi: 10.1016/j.jnucmat.2018.03.016.

[4] Hj. Matzke, « Gas release mechanisms in UO2 - A critical review », *Radiat. Eff.*, vol. 53, p. 219-242, 1980.

[5] J. Rest, M. W. D. Cooper, J. Spino, J. A. Turnbull, P. Van Uffelen, et C. T. Walker, « Fission gas release from UO2 nuclear fuel: A review », *J. Nucl. Mater.*, août 2018, doi: 10.1016/j.jnucmat.2018.08.019.

[6] Turnbull, « The diffusion coefficients of gaseous and volatile species during the irradiation of uranium dioxide », *J. Nucl. Mater.*, vol. 107, p. 168-184, 1982.

[7] J. R. MacEwan et W. H. Stevens, « Xenon Diffusion in UO2 - Some Complicating Factors », *J. Nucl. Mater.*, vol. 11, nº 1, p. 77-93, 1964.

[8] K. N. G. Kaimal, M. C. Naik, et A. R. Paul, « Effect of irradiation and dopant concentration on the migration of xenon in UO2 », *Met. Mater. Process.*, vol. 1, p. 293-300, 1990.

[9] K. N. G. Kaimal, M. C. Naik, et A. R. Paul, « Temperature dependence of diffusivity of xenon in high dose irradiated UO 2 », *J. Nucl. Mater.*, vol. 168, nº 1, p. 188-190, 1989.

[10] W. Miekeley et F. W. Felix, « Effect of stoichiometry on diffusion of xenon in UO2 », *J. Nucl. Mater.*, vol. 42, nº 3, p. 297-306, mars 1972, doi: 10.1016/0022-3115(72)90080-3.

[11] J. Linder et P. Spindler, « Diffusion of Xenon 1300 in UO2 Single Crystals », *Z Naturforschg*, vol. 21a, p. 1723-1725, 1966.

[12] K. Une, K. Nogita, S. Kashibe, et M. Imamura, « Microstructural change and its influence on fission gas release in high burnup UO2 fuel », *J. Nucl. Mater.*, vol. 188, p. 65-72, 1992.

[13] S. Nicoll, H. Matzke, et C. R. A. Catlow, « A computational study of the effect of Xe concentration on the behaviour of single Xe atoms in UO2 », *J. Nucl. Mater.*, vol. 226, nº 1-2, p. 51-57, 1995.

[14] A. H. Booth et G. T. Rymer, « Determination of the Diffusion Constant of Fission Xenon on UO2 Crystals and Sintered Compacts », *AECL-CRDC-720*.

[15] A. B. Auskern, « The diffusion of krypton 85 from uranium dioxide powder », *US Rep. WAPD-TM-185*, 1960.

[16] K. Taketani, « Release of xenon from sintered UO2 at low temperatures ».

[17] D. Davies et G. Long, « The emission of xenon-133 from lightly irradiated uranium dioxide spheroids and powders. », vol. AERE-R 4347, 1963.

[18] A. O. R. Cavaleru, D. G. Armour, et G. Carter, « Thermal evolution spectrometry of low energy inert gas ions injected into polycrystalline UO2 », *Vacuum*, vol. 24, nº 1, p. 13-21, 1973.

[19] M. C. Naik, K. N. G. Kaimal, et M. D. Karkhanavala, « Release of xenon from low-dose irradiated thoria pellets », *J. Nucl. Mater.*, vol. 67, nº 3, p. 239-243, 1977.

[20] J. C. Carter, E. J. Driscoll, et T. S. Elleman, « Xenon-133 diffusion and trapping in single crystal uranium dioxide », *Phys Stat Sol A*, vol. 14, p. 673-680, 1972.

[21] J. H. Evans, A. Van Veen, et K. T. Westerduin, « An investigation into the influence of implanted oxygen on krypton behaviour in uranium dioxide during annealing », *J. Nucl. Mater.*, vol. 208, nº 3, p. 211-218, 1994.

[22] W. H. Stevens et J. R. MacEwan, « The diffusion behavior of fission xenon in uranium dioxide », *At. Energy Can. Ltd. Chalk River Ont. Can.*, 1960.

[23] W. J. Weber, « Thermal recovery of lattice defects in alpha-irradiated UO2 crystals », *J. Nucl. Mater.*, vol. 114, nº 2-3, p. 213-221, 1983.

[24] C. Onofri *et al.*, « Extended defect change in UO2 during in situ TEM annealing », *Acta Mater.*, vol. 196, p. 240-251, sept. 2020, doi: 10.1016/j.actamat.2020.06.038.

[25] C. Onofri, « Étude des défauts étendus induits par irradiation dans UO2 par microscopie électronique en transmission », Université Paul Sabatier, Toulouse, 2016.

[26] « Active Oxide Polishing Suspensions - Brochure ». Struers, 2006.

[27] D. Zipperian, « Colloidal Silica Polishing ». PACE Technologies - Quality Matters Newsletter, 2003.

[28] G. Martin, « Etude et modélisation du comportement sous irradiation de l'hélium dans le dioxyde d'uranium », Orléans, 2007.
[29] M. Fraczkiewicz, « Dopage au chrome du dioxyde d'uranium : Modifications physiques induites », Institut Polytechnique de Grenoble, 2010.
[30] S. Massara et C. Guéneau, « Thermodynamics of Advanced Fuels – International Database », vol. NEA News, nº 32, p. 24, 2014.
[31] J. F. Ziegler, J. P. Biersack, et U. Littmark, « The stopping and Range of Ions in Matter », 2008.
[32] J. Soullard et A. Alamo, « Study on Deceleration of Ions in Diatomic Target », *Radiat. Eff.*, vol. 38, p. 113, 1978.
[33] J. Soullard, « High voltage electron microscope observations of UO2 », *J. Nucl. Mater.*, vol. 135, nº 2-3, p. 190-196, 1985.
[34] A. Michel, « Etude du comportement des gaz de fission dans le dioxyde d'uranium : mécanismes de diffusion, nucléation et grossissement de bulles », Université de Caen Basse-Normandie, 2011.
[35] G. Brindelle, « Etude du relâchement de gaz de fission entrer 600°C et 800°C lors de transitoire thermique sur combustible irradié », Aix-Marseille, 2017.
[36] F. Linez, E. Gilabert, A. Debelle, P. Desgardin, et M.-F. Barthe, « Helium interaction with vacancy-type defects created in silicon carbide single crystal », *J. Nucl. Mater.*, vol. 436, p. 150-157, 2013.
[37] A. Özgümüs, E. Gilabert, N. Dacheux, C. Tamain, B. Lavielle, « Study of radiogenic He diffusion in the β-thorium phosphate diphosphate ceramic », *J. Nucl. Mater.*, vol. 373, p. 112-118, 2008.
[38] A. Sy Ong et S. Elleman, « Effect or trapping in the release of recoil injected gases from solids », *Nucl. Instrum. Methods*, vol. 86, p. 117-125, 1970.
[39] M. V. Speight, « A Calculation on the Migration of Fission Gas in Material Exhibiting Precipitation and Re-solution of Gas Atoms Under Irradiation », *Nucl. Sci. Eng.*, vol. 37, nº 2, p. 180-185, août 1969, doi: 10.13182/NSE69-A20676.
[40] F. S. Ham, « Theory of Diffusion-Limited Precipitation », *J Phys Chem Solids*, vol. 6, p. 335-351, 1958.
[41] R. M. Cornell, M. V. Speight, et B. C. Masters, « The role of bubbles in fission gas release from uranium dioxide », *J. Nucl. Mater.*, vol. 30, nº 1-2, p. 170-178, 1969.
[42] R. J. White et M. O. Tucker, « A new Fission-Gas Release Model », *J. Nucl. Mater.*, vol. 118, p. 1-38, 1983.
[43] P. W. Winter et D. A. MacInnes, « An Analysis of the Thermodynamics of Gas Atoms in very small Bubbles », *J. Nucl. Mater.*, vol. 114, p. 7-14, 1983.
[44] P. T. Elton, P. E. Coleman, et D. A. MacInnes, « A Mechanism for Fission Gas Release from High Temperature Fuel », *J. Nucl. Mater.*, vol. 135, p. 63-67, 1985.
[45] A. Turos, H. Matzke, et S. Kwiatkowski, « Recovery stages in UO2 at low temperatures », *Phys. Rev. Lett.*, vol. 65, nº 10, p. 1215, 1990.
[46] R. Bès *et al.*, « Experimental evidence of Xe incorporation in Schottky defects in UO2 », *Appl. Phys. Lett.*, vol. 106, nº 11, p. 114102, mars 2015, doi: 10.1063/1.4914300.
[47] R. Barnes, « Xenon diffusion in single crystal and sintered UO2 », *Rep. BMI 1533*, 1961.
[48] L. Van Brutzel et M. Rarivomanantsoa, « Molecular dynamics simulation study of primary damage in UO2 produced by cascade overlaps », *J. Nucl. Mater.*, vol. 358, nº 2-3, p. 209-216, nov. 2006, doi: 10.1016/j.jnucmat.2006.07.009.
[49] G. Martin, C. Sabathier, J. Wiktor, et S. Maillard, « Molecular dynamics study of the bulk temperature effect on primary radiation damage in uranium dioxide », *Nucl. Instrum. Methods Phys. Res. Sect. B Beam Interact. Mater. At.*, vol. 352, p. 135-139, juin 2015, doi: 10.1016/j.nimb.2014.12.008.
[50] M. J. Rahman, M. W. D. Cooper, B. Szpunar, et J. A. Szpunar, « Primary radiation damage on displacement cascades in UO2, ThO2 and (U0.5Th0.5)O2 », *Comput. Mater. Sci.*, vol. 154, p. 508-516, nov. 2018, doi: 10.1016/j.commatsci.2018.08.024.
[51] G. Martin *et al.*, « Irradiation-induced heterogeneous nucleation in uranium dioxide », *Phys. Lett. A*, vol. 374, nº 30, p. 3038-3041, juill. 2010, doi: 10.1016/j.physleta.2010.05.033.
[52] M. J. Qin *et al.*, « Thermal conductivity and energetic recoils in UO2 using a many-body potential model », *J. Phys. Condens. Matter*, vol. 26, nº 49, p. 495401, déc. 2014, doi: 10.1088/0953-8984/26/49/495401.

[53] C. Onofri *et al.*, « Changes in voids induced by ion irradiations in UO2: In situ TEM studies », *Nucl. Instrum. Methods Phys. Res. Sect. B Beam Interact. Mater. At.*, vol. 463, p. 76-85, janv. 2020, doi: 10.1016/j.nimb.2019.11.031.
[54] D. A. Andersson, B. P. Uberuaga, P. V. Nerikar, C. Unal, et C. R. Stanek, « U and Xe transport in UO 2 ± x : Density functional theory calculations », *Phys. Rev. B*, vol. 84, nº 5, 2011, doi: 10.1103/PhysRevB.84.054105.
[55] X.-Y. Liu, B. P. Uberuaga, D. A. Andersson, C. R. Stanek, et K. E. Sickafus, « Mechanism for transient migration of xenon in UO2 », *Appl. Phys. Lett.*, vol. 98, p. 151902, 2011.
[56] J.-P. Crocombette, « Ab initio energetics of some fission products (Kr, I, Cs, Sr and He) in uranium dioxide », *J. Nucl. Mater.*, vol. 305, nº 1, p. 29-36, 2002.
[57] M. Freyss, N. Vergnet, et T. Petit, « Ab initio modeling of the behavior of helium and xenon in actinide dioxide nuclear fuels », *J. Nucl. Mater.*, vol. 352, nº 1-3, p. 144-150, juin 2006, doi: 10.1016/j.jnucmat.2006.02.048.
[58] T. Petit *et al.*, « Molecular modelling of transmutation fuels and targets », *J. Nucl. Mater.*, vol. 320, nº 1-2, p. 133-137, juill. 2003, doi: 10.1016/S0022-3115(03)00179-X.
[59] T. Petit, G. Jomard, C. Lemaignan, B. Bigot, et A. Pasturel, « Location of krypton atoms in urnaium dioxide », *J. Nucl. Mater.*, vol. 275, p. 119-123, 1999.
[60] A. E. Thompson et C. Wolverton, « First-principles study of noble gas impurities and defects in UO 2 », *Phys. Rev. B*, vol. 84, nº 13, oct. 2011, doi: 10.1103/PhysRevB.84.134111.
[61] Y. Yun, H. Kim, H. Kim, et K. Park, « Atomic diffusion mechanism of Xe in UO2 », *J. Nucl. Mater.*, vol. 378, nº 1, p. 40-44, août 2008, doi: 10.1016/j.jnucmat.2008.04.013.
[62] Y. Yun, O. Eriksson, P. M. Oppeneer, H. Kim, et K. Park, « First-principales theory for helium and xenon diffusion in uranium dioxide », *J. Nucl. Mater.*, vol. 385, p. 364-367, 2009.
[63] P. V. Nerikar, X.-Y. Liu, B. P. Uberuaga, C. R. Stanek, S. R. Phillpot, et S. B. Sinnott, « Thermodynamics of fission products in UO2±x », *J. Phys. Condens. Matter*, vol. 21, nº 43, p. 435602, oct. 2009, doi: 10.1088/0953-8984/21/43/435602.
[64] E. Vathonne *et al.*, « Determination of Krypton Diffusion Coefficients in Uranium Dioxide Using Atomic Scale Calculations », *Inorg. Chem.*, vol. 56, nº 1, p. 125-137, janv. 2017, doi: 10.1021/acs.inorgchem.6b01560.
[65] D. A. Andersson *et al.*, « Atomistic modeling of intrinsic and radiation-enhanced fission gas (Xe) diffusion in UO2±x : Implications for nuclear fuel performance modeling », *J. Nucl. Mater.*, vol. 451, nº 1-3, p. 225-242, août 2014, doi: 10.1016/j.jnucmat.2014.03.041.
[66] R. W. Grimes et C. R. A. Catlow, « The Stability of Fission Products in Uranium Dioxide », *Philos. Trans. R. Soc. Math. Phys. Eng. Sci.*, vol. 335, nº 1639, p. 609-634, juin 1991, doi: 10.1098/rsta.1991.0062.
[67] K. Govers, S. E. Lemehov, et M. Verwerft, « On the solution and migration of single Xe atoms in uranium dioxide – An interatomic potentials study », *J. Nucl. Mater.*, vol. 405, nº 3, p. 252-260, oct. 2010, doi: 10.1016/j.jnucmat.2010.08.013.
[68] S. T. Murphy, A. Chartier, L. Van Brutzel, et J.-P. Crocombette, « Free energy of Xe incorporation at point defects and in nanovoids and bubbles in UO 2 », *Phys. Rev. B*, vol. 85, nº 14, avr. 2012, doi: 10.1103/PhysRevB.85.144102.
[69] M. W. D. Cooper, C. R. Stanek, J. A. Turnbull, B. P. Uberuaga, et D. A. Andersson, « Simulation of radiation driven fission gas diffusion in UO 2 , ThO 2 and PuO 2 », *J. Nucl. Mater.*, vol. 481, p. 125-133, déc. 2016, doi: 10.1016/j.jnucmat.2016.09.013.
[70] P. Garcia *et al.*, « A study of xenon aggregates in uranium dioxide using X-ray absorption spectroscopy », *J. Nucl. Mater.*, vol. 352, nº 1-3, p. 136-143, juin 2006, doi: 10.1016/j.jnucmat.2006.02.047.
[71] P. Martin *et al.*, « XAS characterisation of xenon bubbles in uranium dioxide », *Nucl. Instrum. Methods Phys. Res. Sect. B Beam Interact. Mater. At.*, vol. 266, nº 12-13, p. 2887-2891, juin 2008, doi: 10.1016/j.nimb.2008.03.180.
[72] P. M. Martin *et al.*, « Behavior of fission gases in nuclear fuel: XAS characterization of Kr in UO2 », *J. Nucl. Mater.*, vol. 466, p. 379-392, nov. 2015, doi: 10.1016/j.jnucmat.2015.08.019.
[73] D. Pizzocri *et al.*, « A model describing intra-granular fission gas behaviour in oxide fuel for advanced engineering tools », *J. Nucl. Mater.*, vol. 502, p. 323-330, avr. 2018, doi: 10.1016/j.jnucmat.2018.02.024.